A Treatise on Potential Energy Diagrams in Physics

A Historical and Pedagogical Review

Onri Jay Benally

August 2025

The Landscape of Possibility

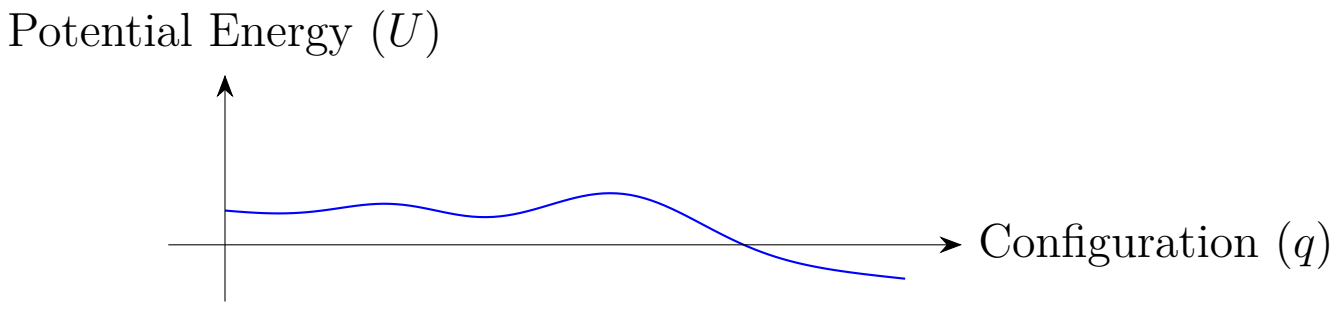

Contents

1 Introduction: The Enduring Metaphor of the Hill

In the long arc of physics, thinkers have repeatedly sketched "hills" and "walls" of potential energy so that our eyes—and therefore our intuition—can follow how a particle, charge-carrier, or chemical complex might move. This visual metaphor, rooted in our everyday experience with gravity, has proven to be remarkably versatile and enduring. Starting with gravity-like drawings for springs and projectiles, progressing through chemical "activation hills," quantum-mechanical tunneling barriers, semiconductor band steps, and today's tilted-washboard landscapes for Josephson circuits, the diagram style has steadily evolved, yet the underlying concept has stayed the same: a vertical axis of energy, a horizontal axis of configuration, and arrows that announce motion "up-and-over" or, more subtly, "through" the barrier when quantum physics allows.

The power of this diagrammatic approach lies in its ability to translate abstract mathematical relationships into a tangible, graphical landscape. The shape of a curve on a page immediately conveys concepts of stability, transition, and confinement that would otherwise require pages of equations to describe. It is a tool for both pedagogy and research, allowing students to build intuition and experts to frame complex problems.

This document explores the history, application, and pedagogical power of the potential energy diagram. We will begin with a primer suitable for early students, tracing the core analogy to a simple gravitational hill. We will then embark on a more expansive graduate-level analysis, examining the key historical milestones where this diagrammatic tool was adapted to new domains of physics, from chemical kinetics to quantum computing. We will introduce new diagrams to illustrate these advanced concepts, delve into the mathematical formalism that underpins them, and present a series of tables and conceptual maps to summarize the evolution of these conventions. The goal is to create a comprehensive reference on this foundational tool of theoretical physics, demonstrating its breadth and its continued relevance in modern science.

2 A Brief Primer

At its heart, the potential energy diagram is a simple idea that leverages our intuition about the physical world. The core concepts can be grasped with four key points, each building on the last.

2.1 Energy Hills Act Like Gravity Hills

When you see a hump on a potential-energy graph, imagine trying to push a ball over an earthly hill. Gravity resists your effort, so you must supply extra push, which translates to kinetic energy. In the diagram, that "extra push" is the energy difference between the particle's total energy and the peak of the potential hill. If the particle's energy is greater than the hill's peak, it rolls over; if not, it rolls back. This simple, powerful analogy is often the first introduction students have to the concept for systems like springs, planets, and electrons, precisely because the connection to gravity is so familiar and intuitive. In this one-dimensional case, the horizontal axis x is a simple configuration coordinate; later we will generalize to a vector of coordinates $\mathbf{q}$ that jointly describe a system's configuration space.

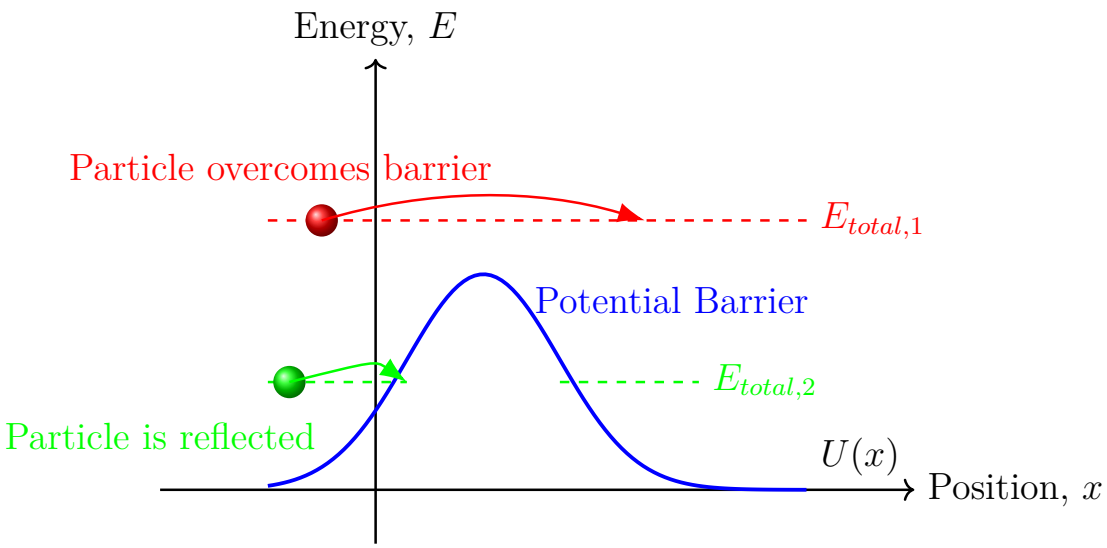

Figure 1: A classical potential energy hill. A particle with total energy $E_{total,1}$ (red) can pass over the barrier, while a particle with energy $E_{total,2}$ (green) is confined to the region left of the hill.

2.2 Barriers in Chemistry Play the Same Role

The analogy extends directly to chemistry. For a chemical reaction to occur, reactant molecules must collide with sufficient energy to overcome an energetic barrier and rearrange into products. This minimum energy is called the **activation energy** (E_a), a concept famously captured by the Arrhenius equation in 1889. For many thermally activated processes the empirical rate law can be written as

$$k(T) = A \exp\left(-\frac{E_a}{RT}\right),$$

which makes the energetic hill appear directly in the exponential suppression factor. A reaction coordinate diagram, which plots energy versus the progress of a reaction, shows this activation energy as a hill that separates reactants from products.

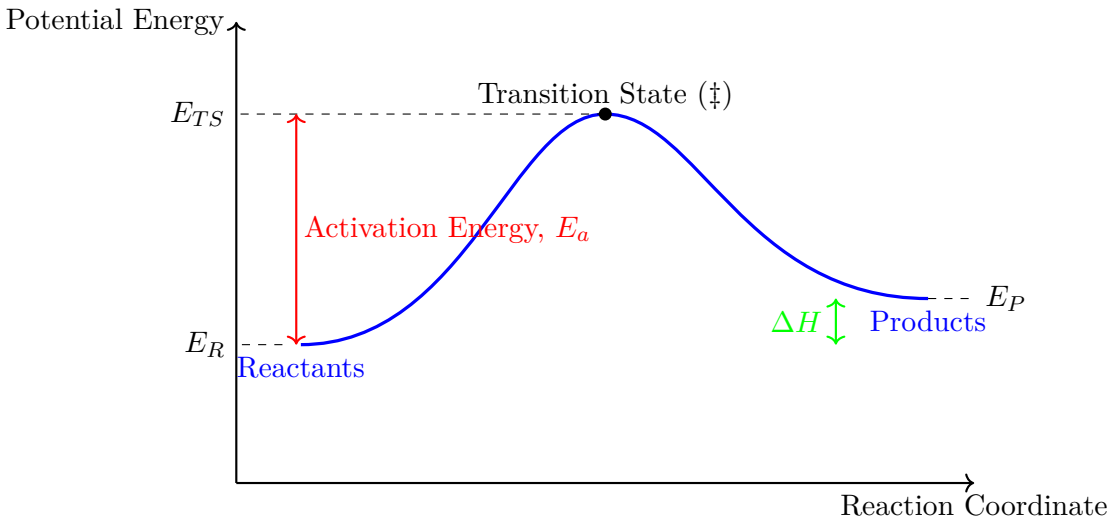

Figure 2: A reaction coordinate diagram for an endothermic reaction. Reactants must gain the activation energy (E_a) to reach the transition state before forming products. The overall change in enthalpy (ΔH) is positive.

2.3 Quantum Particles Sometimes "Cheat"

The classical world is deterministic in this regard: not enough energy means you cannot cross. The quantum world, however, is probabilistic. In 1928, George Gamow explained the phenomenon of alpha decay by showing that an alpha particle can **tunnel through** a nuclear potential barrier even if it classically lacks the energy to go over it. This revolutionary idea meant that arrows in quantum diagrams could now slice straight through the wall, representing a classically forbidden process made possible by the wave-like nature of particles. Mathematically, in a region where $U(x) > E$ the time-independent Schrödinger equation implies a solution of the form $\psi(x) \propto \exp[-\kappa x]$ with $\kappa > 0$, so the probability density decays inside the barrier yet remains non-zero on the far side.

2.4 Modern Chips Still Draw Hills

The hill metaphor remains central in cutting-edge technology. In superconducting quantum bits (qubits), the state of the system is described by the phase of a quantum wavefunction, which sits in a potential energy landscape. For a Josephson junction, this landscape is often a "tilted washboard" potential. Engineers can tune an external bias current to tilt this washboard, effectively lowering or raising the hills between adjacent wells, which allows them to control the quantum state of the qubit. This will be explored in detail in Sections 4.7 and 4.

3 Graduate-Level Analysis: A Historical Trajectory

The potential energy diagram is not a static concept but one that has been refined and repurposed over nearly two centuries of physics. Its evolution tracks the major theoretical developments in the field.

3.1 Classical and Early Analytical Mechanics (1740 – 1870)

While the concept of potential energy was formalized by Lagrange in his *Mécanique analytique*, the initial formulations were purely algebraic. Early thinkers like Bernoulli and Lagrange worked with expressions of kinetic minus potential energy ($T - U$) without the aid of graphical representation.

It was not until the mid-19th century that textbook authors, notably William Rankine and later James Clerk Maxwell, began to plot potential energy $U(x)$ against a configuration coordinate x. These early diagrams were used to illustrate fundamental concepts such as stable and unstable equilibrium points and the nature of simple harmonic motion. A particle placed at a local minimum of a potential well would oscillate, while a particle placed at a maximum would be in unstable equilibrium, ready to roll down the hill. This marked the birth of the potential energy diagram as a pedagogical tool.

3.2 Chemical Kinetics and the "Activation Hill" (1884 – 1930)

The application of energy diagrams to chemistry began with the work of Jacobus Henricus van 't Hoff and Svante Arrhenius. By studying the temperature dependence of reaction rates, they inferred that most reactions face a fixed energy obstacle. Arrhenius proposed his famous equation,

$$k = Ae^{-E_a/(RT)} \tag{1}$$

where k is the reaction rate constant, A is a pre-exponential factor, R is the gas constant, T is the absolute temperature, and E_a is the activation energy. This equation mathematically

described the "hill" that reactants must climb.

This picture was formalized in 1935 with the development of **Transition State Theory (TST)** by Henry Eyring, Meredith Gwynne Evans, and Michael Polányi. TST posits that a quasi-equilibrium exists between reactants and an activated complex at the peak of the energy barrier, known as the transition state. Diagrams from this era are often marked with a double dagger (‡) at the peak to signify this special configuration, as shown previously in Figure 2.

3.3 Quantum Tunneling Barriers (1928 – 1950)

The classical paradigm of insurmountable barriers was shattered with the advent of quantum mechanics. The puzzle of alpha decay—how an alpha particle could escape the strong nuclear force holding it within a nucleus—was solved independently by George Gamow and by Ronald Gurney and Edward Condon in 1928. They modeled the nucleus as a potential well surrounded by a high Coulomb barrier. Classically, an alpha particle with an energy below the barrier peak would be trapped forever. Quantum mechanically, however, the particle's wavefunction does not abruptly go to zero at the barrier wall. Instead, it decays exponentially inside the barrier. If the barrier is thin enough, the wavefunction has a small but non-zero amplitude on the other side, implying a finite probability of escape. This phenomenon was named **quantum tunneling**.

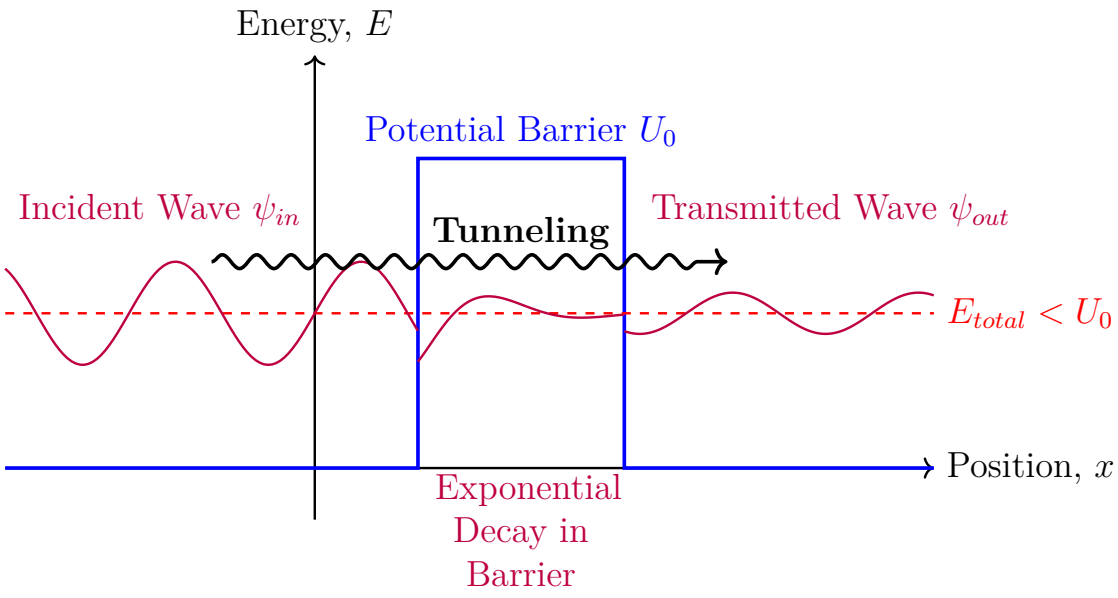

Figure 3: Quantum tunneling through a potential barrier. The particle's wavefunction (purple) has a non-zero amplitude after the barrier, indicating a probability of transmission even though its energy E_{total} is less than the barrier height U_0.

The mathematical basis for this is the time-independent Schrödinger equation:

$$-\frac{\hbar^2}{2m}\frac{d^2\psi(x)}{dx^2} + U(x)\psi(x) = E\psi(x) \tag{2}$$

In a classically forbidden region where $U(x) > E$, the solution for $\psi(x)$ is no longer oscillatory but takes the form of a real exponential decay. The semi-classical **Wentzel–Kramers–Brillouin (WKB)** approximation provided a powerful tool for calculating tunneling probabilities for barriers of arbitrary shape.

3.4 Semiconductor Band & Junction Diagrams (1930 – present)

A parallel evolution of energy diagrams occurred in solid-state physics. The quantum theory of solids, developed in the 1930s, introduced the concept of electronic **band structure**. When two different types of semiconductors (p-type and n-type) are brought together to form a p-n junction, the band energies must align to create a constant Fermi level, resulting in **band bending**. This creates a potential barrier at the junction that is essential for the rectifying behavior of diodes. The gravitational analogy persists here: electrons are said to "roll downhill" from high conduction-band edges to low ones.

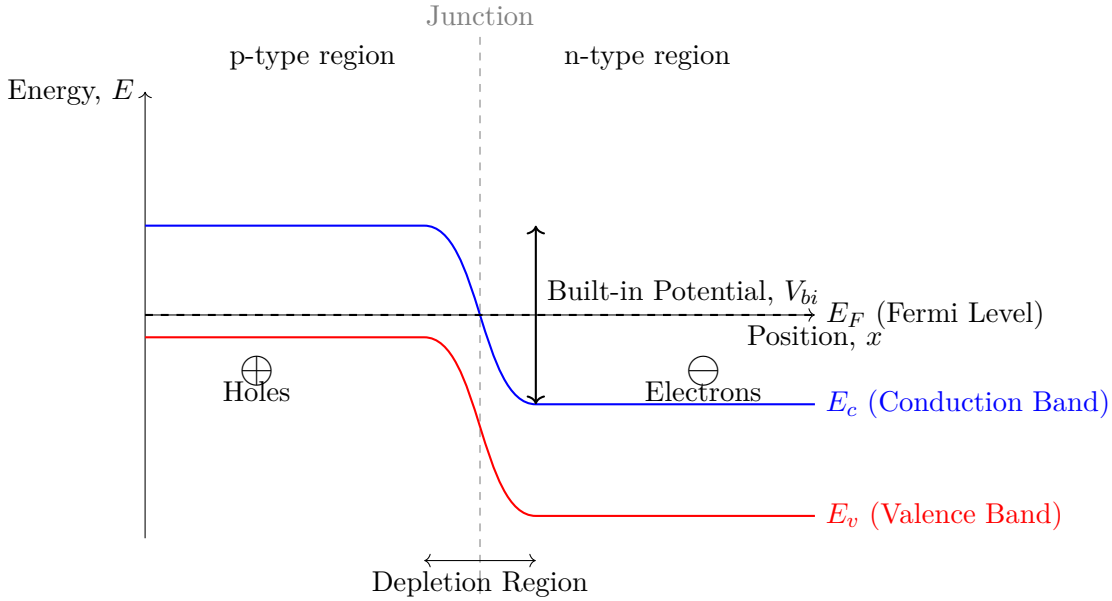

Figure 4: A band diagram for a p-n junction at equilibrium. Band bending creates a potential barrier that prevents the net flow of charge carriers across the junction.

For a quantitative link to dopants, permittivity, and barrier width, see Section 4.6.

3.5 Macroscopic Quantum Devices (1980 – present)

In the late 20th century, physicists began to build devices where macroscopic variables behave quantum mechanically. A prime example is the **Josephson junction**, formed by two superconductors separated by a thin insulating layer. The dynamics of the quantum phase difference ϕ across the junction can be described by a particle moving in a potential given by:

$$U(\phi) = -E_J \cos(\phi) - \frac{\hbar I_b}{2e}\phi \tag{3}$$

where E_J is the Josephson energy and I_b is an external bias current. This is famously known as the **tilted-washboard potential**. By adjusting the tilt (I_b), one can trap the "phase particle" in a well or allow it to escape, forming the basis of superconducting qubits.

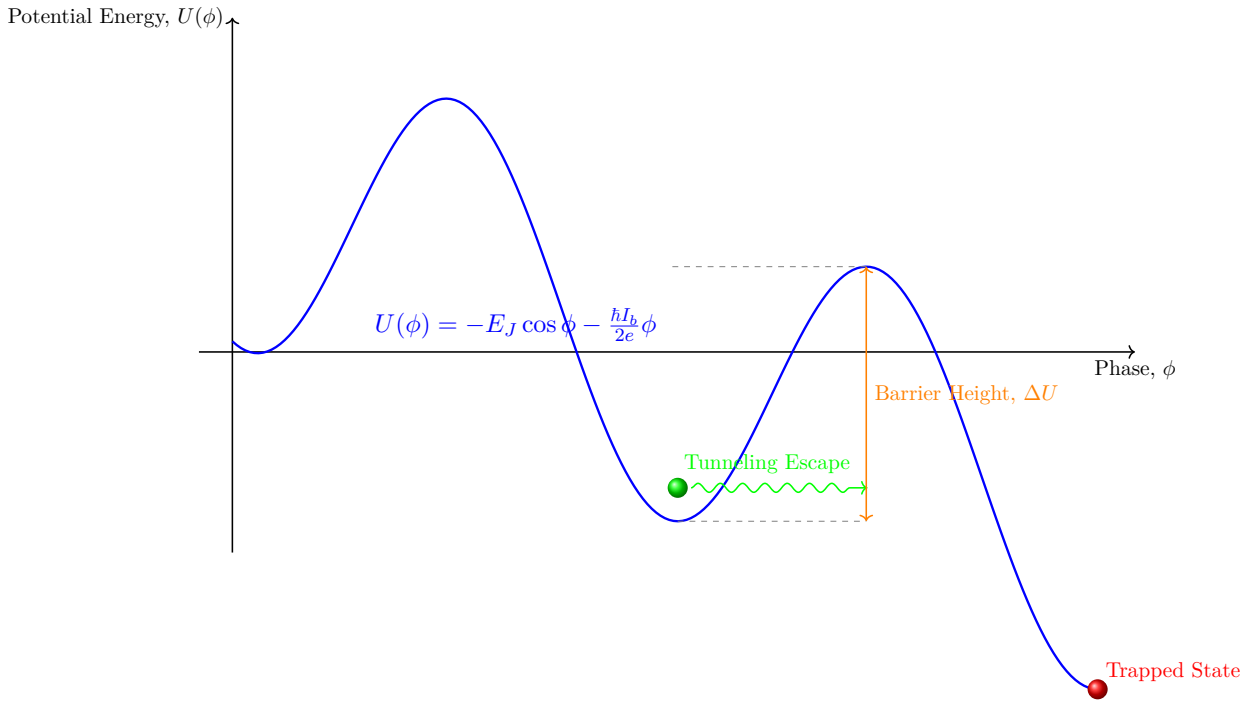

Figure 5: The tilted-washboard potential for a Josephson junction. A quantum state can be trapped in a potential well or can escape via quantum tunneling. The barrier height ΔU is shown relative to the well from which tunneling occurs.

For the full RCSJ dynamics, plasma frequency, and barrier-height formula $\Delta U(i)$, see Section 4.7.

4 Mathematical Formalism and Stability Analysis

Because intuition benefits from precise anchors, and because diagrams deserve equations that certify the picture, we now set the rigorous footing. Throughout, e denotes the elementary charge, $\hbar = h/2\pi$, k_{B} is Boltzmann's constant, and $\Phi_0 = h/2e$.

Standing assumptions. Unless otherwise stated, we take the configuration space to be $\mathbb{R}^n$ with generalized coordinates $\mathbf{q}$; the potential $U : \mathbb{R}^n \to \mathbb{R}$ is at least twice continuously differentiable (C^2); the force field is conservative, $\mathbf{F}(\mathbf{q}) = -\nabla U(\mathbf{q})$; and any mass matrix M that appears is symmetric positive definite. These mild smoothness and positivity assumptions are enough to justify the Hessian-based stability classification and normal-mode analysis that follow.

4.1 Force–Potential Relations in One and Many Dimensions

In one dimension, a conservative force is the negative slope of the potential:

$$F(x) = -\frac{dU(x)}{dx}. \tag{4}$$

In n dimensions with generalized coordinates $\mathbf{q} \in \mathbb{R}^n$,

$$\mathbf{F}(\mathbf{q}) = -\nabla U(\mathbf{q}), \qquad \nabla = \begin{bmatrix} \partial/\partial q_1 & \cdots & \partial/\partial q_n \end{bmatrix}^{\top}. \tag{5}$$

4.2 Equilibria, Hessian, and Stability (Morse Classification)

Equilibria satisfy $\nabla U(\mathbf{q}_*) = \mathbf{0}$. The second-derivative matrix,

$$H(\mathbf{q}_*) = \nabla^2 U(\mathbf{q}_*) \in \mathbb{R}^{n \times n}, \tag{6}$$

classifies the equilibrium:

- **Strict local minimum (nonlinear Lyapunov stable):** H positive definite (all

eigenvalues > 0).

- **Saddle:** H indefinite (one or more negative eigenvalues); the number of negative eigenvalues is the *Morse index*.
- **Local maximum (unstable):** H negative definite (all eigenvalues < 0).

For a conservative mechanical system with kinetic energy $T = \frac{1}{2}\dot{\mathbf{q}}^\top M \dot{\mathbf{q}}$ and potential U, the total energy $E = T + U$ is a Lyapunov function. If $H(\mathbf{q}_*)$ is positive definite, then $\mathbf{q}_*$ is a strict local energy minimum and therefore Lyapunov stable; saddles and maxima are locally energetically unstable. Under the smoothness assumptions above, nondegenerate critical points (those with $\det H(\mathbf{q}_*) \neq 0$) are Morse critical points; the Morse index is exactly the number of negative eigenvalues of $H(\mathbf{q}_*)$.

4.3 Small Oscillations and Normal Modes

Near a stable equilibrium $\mathbf{q}_*$, write $\mathbf{q} = \mathbf{q}_* + \boldsymbol{\eta}$. With kinetic energy $T = \frac{1}{2}\dot{\boldsymbol{\eta}}^\top M \dot{\boldsymbol{\eta}}$ (constant mass matrix M evaluated at $\mathbf{q}_*$) and $U(\mathbf{q}) \approx U(\mathbf{q}_*) + \frac{1}{2}\boldsymbol{\eta}^\top H \boldsymbol{\eta}$, the linearized equations become

$$M\,\ddot{\boldsymbol{\eta}} + H\,\boldsymbol{\eta} = \mathbf{0}. \tag{7}$$

Seeking $\boldsymbol{\eta}(t) = \mathbf{v}\,e^{i\omega t}$ yields the generalized eigenproblem

$$H\,\mathbf{v} = \omega^2 M\,\mathbf{v}, \tag{8}$$

so the normal-mode frequencies are $\omega_i = \sqrt{\lambda_i}$ where λ_i are the generalized eigenvalues of (H, M). Because M is symmetric positive definite and H is symmetric, one can always transform to mass-weighted normal coordinates that diagonalize the quadratic forms, so the motion decomposes into independent harmonic oscillators.

4.4 Semiclassical Tunneling (Wentzel–Kramers–Brillouin)

For a 1D barrier with turning points $a < b$ and energy E, the WKB transmission is

$$T \approx \exp\!\left(-2\int_a^b \kappa(x)\,dx\right), \qquad \kappa(x) = \frac{\sqrt{2m\,[U(x)-E]}}{\hbar}, \tag{9}$$

valid when the de Broglie wavelength varies slowly, for example when $\left|\frac{1}{\kappa^2}\frac{d\kappa}{dx}\right| \ll 1$. In that semiclassical regime the WKB method gives an asymptotic expansion in powers of $\hbar$; the expression above should be read as the leading exponential factor, with turning-point connection formulas providing prefactors. In multiple dimensions, the integral is replaced by a bounce (instanton) action in imaginary time.

Example (square barrier estimate). Consider an electron of mass m_e incident on a square barrier of height $U_0 = 1\,\mathrm{eV}$ and width $L = 0.5\,\mathrm{nm}$ with kinetic energy $E = 0.2\,\mathrm{eV}$. For this simple case κ is constant inside the barrier, $\kappa = \sqrt{2m_e(U_0 - E)}/\hbar$, and the WKB estimate reduces to $T \approx \exp(-2\kappa L)$. Using standard constants, this gives $T \sim 10^{-2}$, that is, a transmission probability of order one percent per attempt, showing how an apparently formidable barrier can still be crossed occasionally by tunneling.

4.5 Transition-State Theory (TST) and Kramers Escape

On a multi-dimensional potential energy surface (PES), the *transition state* is a saddle with exactly one unstable direction. Canonical TST gives the rate

$$k_{\mathrm{TST}} = \frac{k_{\mathrm{B}}T}{h}\,\frac{Q^{\ddagger}}{Q_{\mathrm{R}}}\,\exp\!\left(-\frac{\Delta G^{\ddagger}}{k_{\mathrm{B}}T}\right), \tag{10}$$

with $Q^{\ddagger}$ the partition function restricted to the dividing surface and Q_{R} that of reactants, and with $\kappa \le 1$ often included as a multiplicative transmission coefficient to account for recrossings. TST implicitly assumes quasi-equilibrium between reactants and the transition-

state region and a dividing surface chosen to minimize reactive-trajectory recrossings.

For thermally activated barrier crossing in a 1D potential $U(x)$ subject to viscous drag γ (overdamped Langevin limit), Kramers' high-friction rate is

$$k \approx \frac{\omega_0\,\omega_b}{2\pi\gamma}\,\exp\!\left(-\frac{\Delta U}{k_{\mathrm{B}}T}\right), \tag{11}$$

where $\omega_0^2 = U''(x_{\min})/m$ at the well minimum and $\omega_b^2 = |U''(x_{\mathrm{barrier}})|/m$ at the barrier top. This expression arises from a Langevin dynamics with friction coefficient γ and Gaussian white noise consistent with a thermal bath at temperature T. In the underdamped regime, prefactors differ but the Arrhenius exponential persists.

4.6 Electrostatics of a p–n Junction: Built-in Potential and Width

Let $x = 0$ be the metallurgical junction, with acceptor density N_A on $x < 0$ and donor density N_D on $x > 0$. In the depletion approximation, Poisson's equation

$$\frac{d^2\varphi}{dx^2} = -\frac{\rho(x)}{\varepsilon_s} = \begin{cases} +\dfrac{eN_A}{\varepsilon_s}, & -x_p < x < 0, \\ -\dfrac{eN_D}{\varepsilon_s}, & 0 < x < x_n, \\ 0, & \text{otherwise}, \end{cases} \tag{12}$$

with charge neutrality $N_A x_p = N_D x_n$, integrates to the built-in potential and depletion width

$$V_{bi} = \frac{k_{\mathrm{B}}T}{e}\,\ln\!\left(\frac{N_A N_D}{n_i^2}\right), \qquad W = x_p + x_n = \sqrt{\frac{2\varepsilon_s V_{bi}}{e}\left(\frac{1}{N_A} + \frac{1}{N_D}\right)}. \tag{13}$$

Here ε_s is the semiconductor permittivity and $e > 0$ is the magnitude of the elementary charge; the signs of the space-charge density are carried by the explicit $\pm$ signs in Poisson's equation. Within the depletion approximation we neglect mobile carriers in $-x_p < x < x_n$ and treat the ionized dopant densities N_A and N_D as uniform.

Example (numerical silicon junction). Consider a silicon p–n junction at $T = 300\,\mathrm{K}$ with $N_A = N_D = 10^{16}\,\mathrm{cm}^{-3}$ (that is, $10^{22}\,\mathrm{m}^{-3}$), intrinsic carrier concentration $n_i \approx 1.5 \times 10^{10}\,\mathrm{cm}^{-3}$, and $\varepsilon_s \approx 11.7\,\varepsilon_0$ where ε_0 is the vacuum permittivity. The formulas above give $V_{bi} \approx 0.7$ V and a total depletion width $W \approx 0.4\ \mu$m, both in line with standard order-of-magnitude estimates from device-physics textbooks.

These relations tie the band diagram's "hill" height and width in Fig. 4 to dopant densities and the semiconductor permittivity.

4.7 Josephson Junction Dynamics: RCSJ Model, Plasma Frequency, and Escape

For a current-biased junction with capacitance C and shunt resistance R, the Resistively and Capacitively Shunted Junction (RCSJ) equation for the superconducting phase difference ϕ is

$$C\left(\frac{\Phi_0}{2\pi}\right)\ddot{\phi} \;+\; \frac{1}{R}\left(\frac{\Phi_0}{2\pi}\right)\dot{\phi} \;+\; I_c \sin\phi \;=\; I_b + \xi(t), \tag{14}$$

equivalent to a particle of effective mass $m_{\mathrm{eff}} = C(\Phi_0/2\pi)^2$ moving in

$$U(\phi) = -E_J \cos\phi - \frac{\hbar I_b}{2e}\,\phi, \qquad E_J = \frac{\hbar I_c}{2e}, \tag{15}$$

the "tilted-washboard" (see Fig. **??**). Writing $i = I_b/I_c$, the small-oscillation (plasma) frequency at a well bottom and the barrier height to the adjacent saddle are

$$\omega_p(i) = \sqrt{\frac{2eI_c}{\hbar C}}\,(1-i^2)^{1/4}, \qquad \Delta U(i) = 2E_J\Big[\sqrt{1-i^2} - i\,\arccos(i)\Big]. \tag{16}$$

Here $\xi(t)$ represents a stochastic current from the thermal environment, typically modeled as Gaussian white noise with $\langle \xi(t)\rangle = 0$ and $\langle \xi(t)\xi(t')\rangle \propto (k_{\mathrm{B}}T/R)\,\delta(t-t')$, consistent with the fluctuation–dissipation theorem. Thermally activated escape follows Kramers-like forms with ω_p as the attempt frequency; at sufficiently low T, macroscopic quantum tunneling

replaces thermal activation.

4.8 Landau Expansions and Saddle-Point Structure Near Symmetry Breaking

Near a continuous phase transition, a scalar order parameter ψ often admits

$$U(\psi) = a\,(T - T_c)\,\psi^2 + b\,\psi^4 + \cdots, \quad b > 0, \tag{17}$$

so that for $T > T_c$ the minimum is at $\psi = 0$, while for $T < T_c$ the minima bifurcate to $\psi = \pm\sqrt{-a(T - T_c)/2b}$. The Hessian at $\psi = 0$ changes sign at T_c, cleanly connecting curvature to stability and to the emergence of multiple wells.

4.9 Minimum-Energy Paths on Multidimensional Surfaces (NEB Sketch)

To locate an energetically favorable pathway between minima on a PES, the Nudged Elastic Band (NEB) method relaxes a discrete string of images $\{\mathbf{R}_i\}$ under forces decomposed into parallel and perpendicular components with respect to the path tangent, schematically

$$\mathbf{F}_i^{\mathrm{NEB}} \;=\; -\nabla U(\mathbf{R}_i)\Big|_{\perp} \;+\; k\Big(\|\mathbf{R}_{i+1} - \mathbf{R}_i\| - \|\mathbf{R}_i - \mathbf{R}_{i-1}\|\Big)\,\hat{\boldsymbol{\tau}}_i\Big|_{\parallel}, \tag{18}$$

thereby finding the minimum-energy path that crosses a first-order saddle (the transition state). Here $\hat{\boldsymbol{\tau}}_i$ is a unit tangent vector to the discretized path at image i, so $(\cdot)_\perp$ and $(\cdot)_\parallel$ denote projections perpendicular and parallel to $\hat{\boldsymbol{\tau}}_i$, respectively. In climbing-image variants the highest-energy image is further modified so that it converges directly to the saddle point.

5 Evolution of Diagrammatic Conventions

The potential energy diagram has adapted its form to suit the physics of each era. While the core concept remains, the details of what is plotted and what is represented have changed significantly. The table below summarizes this evolution, highlighting the key features of the diagrams used in different fields and historical periods. This summary provides a bird's-eye view of the intellectual lineage of this powerful visual tool.

Table 1: A Timeline of Potential Energy Diagram Conventions

Era	**Typical Abscissa (Horizontal Axis)**	**Barrier Style**	**Motion Indicator**	**Key Concept/ Reference**
1850s	Position (x)	Smooth, generic hill	Arrow drawn over the top of the hill	Maxwell's illustrations of stability and oscillation.
1889	Reaction coordinate	Single, sharp peak representing the transition state	Arrow rising from reactants to peak, then falling to products	Arrhenius equation and the concept of activation energy (E_a).
1928	Radial distance in nucleus (r)	Square well plus a decaying Coulomb wall	Arrow pointing directly *through* the barrier wall	Gamow's theory of alpha decay and quantum tunneling.
1935	Reaction coordinate	A saddle point on a multi-dimensional surface	A curved path or trajectory over the saddle point	Transition State Theory (TST) formalizing the activated complex (‡).
1947	Depth into a semiconductor device	Abrupt steps or gradual bending of energy bands	Arrows indicating electron and hole flow (downhill/uphill)	Early p-n junction and transistor band diagrams.

Continued on next page

Table 1 – continued from previous page

Era	**Typical Abscissa (Horizontal Axis)**	**Barrier Style**	**Motion Indicator**	**Key Concept/ Reference**
1985	Superconducting phase difference (ϕ)	Tilted periodic cosine wave ("washboard")	Arrows showing escape from a potential well	Josephson junction dynamics for qubits and SQUIDs.
2010s	Multi-dimensional Potential Energy Surface (PES)	Color-mapped ridges and valleys on a 2D or 3D plot	Streamlines, tunneling paths, or probability density plots	Modern computational chemistry and quantum dynamics visualizers.

6 Conceptual Connections and Glossary

To synthesize the information, we can visualize the connections between these ideas with a mind map and define the key acronyms in a glossary.

6.1 Mind-Map of Concepts

The various applications of energy diagrams can be organized into a conceptual tree, showing how the core idea has branched into different domains of physics.

[Figures are on the next page...]

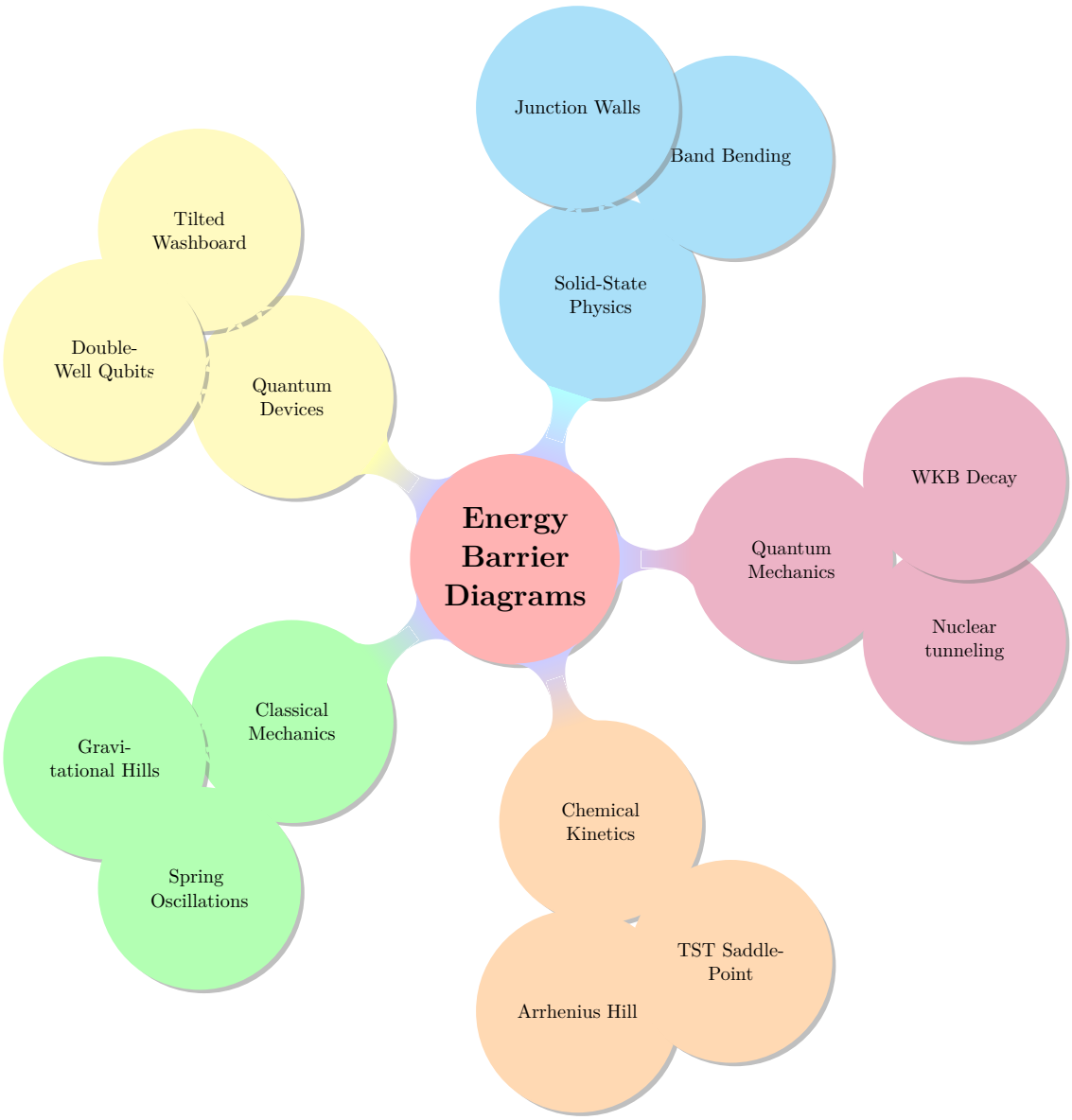

Figure 6: A mind-map illustrating the branching applications of potential energy diagrams across different fields of physics.

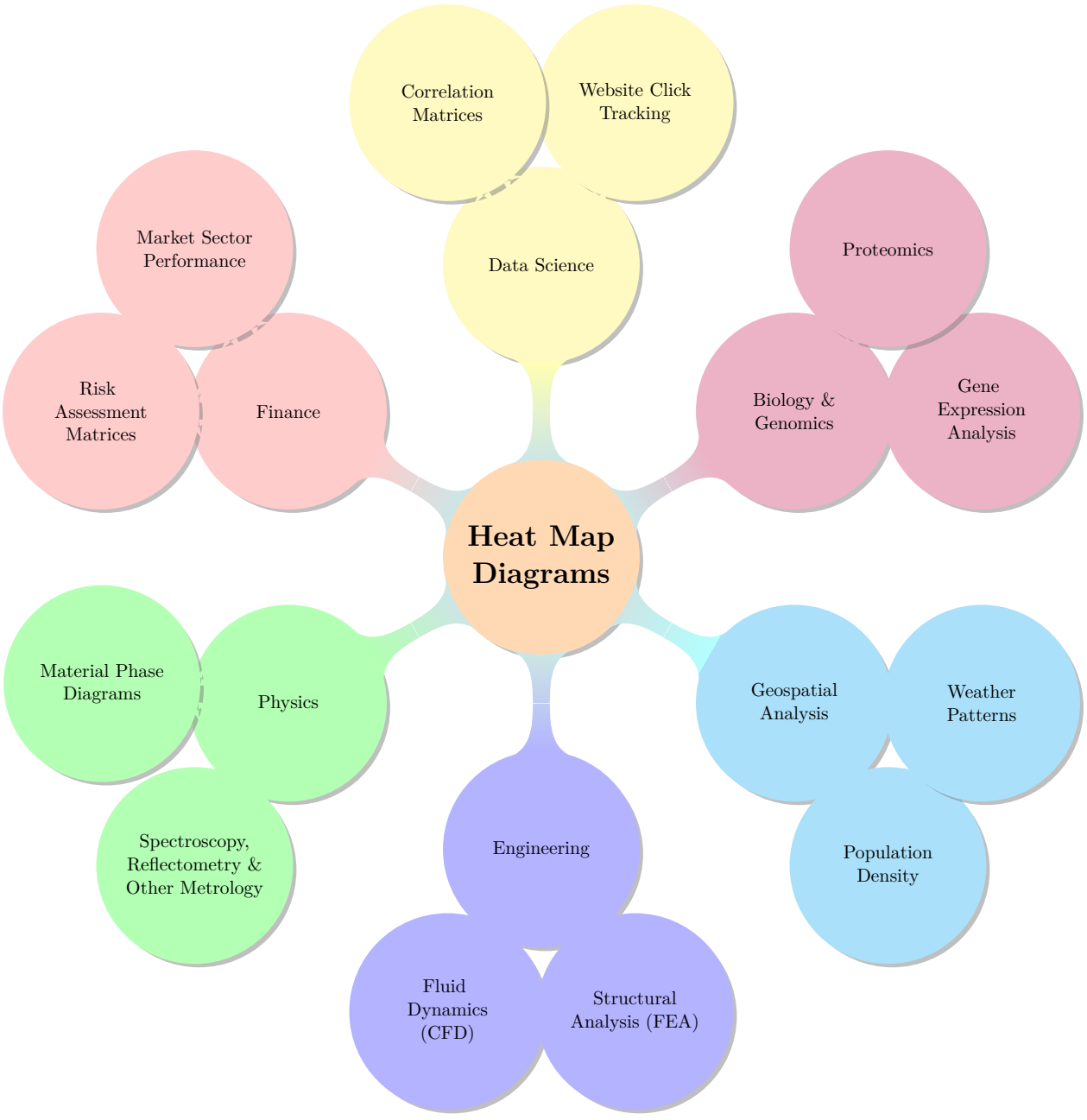

Figure 7: An additional mind-map illustrating the broad, cross-disciplinary applications of heat map diagrams.

7 Formula Sheet: Barriers, Rates, and Wells

Table 2: Frequently Used Relations for Potential Energy Barriers and Stability

Topic	**Formula**	**Notes/ Definitions**
Force–potential (1D)	$F(x) = -\,dU/dx$	Conservative force points downhill
Force–potential (ND)	$\mathbf{F}(\mathbf{q}) = -\,\nabla U(\mathbf{q})$	$\mathbf{q} \in \mathbb{R}^n$
Equilibrium condition	$\nabla U(\mathbf{q}_*) = \mathbf{0}$	Critical points of U
Stability classification	$H = \nabla^2 U(\mathbf{q}_*)$; sign of eigenvalues $\Rightarrow$ min / saddle / max	Morse index = # negative eigenvalues
Small oscillations	$M\ddot{\boldsymbol{\eta}} + H\boldsymbol{\eta} = 0, \quad H\mathbf{v} = \omega^2 M\mathbf{v}$	Normal modes near a minimum
WKB transmission	$T \approx \exp\Big[-2\int_a^b \sqrt{2m\,[U(x)-E]}\,dx/\hbar\Big]$	Valid when $\left\lvert\frac{1}{\kappa^2}\frac{d\kappa}{dx}\right\rvert \ll 1$
TST (Eyring)	$k = \dfrac{k_{\mathrm{B}}T}{h}\,\dfrac{Q^{\ddagger}}{Q_{\mathrm{R}}}\,e^{-\Delta G^{\ddagger}/k_{\mathrm{B}}T}$	$\kappa \le 1$ corrects recrossings
Kramers (overdamped)	$k \approx \dfrac{\omega_0\,\omega_b}{2\pi\gamma}\,e^{-\Delta U/k_{\mathrm{B}}T}$	$\omega_0^2 = U''(x_{\min})/m$, $\omega_b^2 = \lvert U''(x_{\mathrm{barrier}})\rvert/m$
p–n built-in potential	$V_{bi} = \dfrac{k_{\mathrm{B}}T}{e}\ln\!\Big(\dfrac{N_A N_D}{n_i^2}\Big)$	Depletion approximation
p–n depletion width	$W = \sqrt{\dfrac{2\varepsilon_s V_{bi}}{e}\Big(\dfrac{1}{N_A}+\dfrac{1}{N_D}\Big)}$	$N_A x_p = N_D x_n$
JJ potential (biased)	$U(\phi) = -E_J\cos\phi - \dfrac{\hbar I_b}{2e}\phi, \quad E_J = \dfrac{\hbar I_c}{2e}$	Tilted washboard
JJ plasma frequency	$\omega_p(i) = \sqrt{\dfrac{2eI_c}{\hbar C}}\,(1-i^2)^{1/4}, \quad i = I_b/I_c$	Small oscillations at well bottom
JJ barrier height	$\Delta U(i) = 2E_J\Big[\sqrt{1-i^2} - i\,\arccos(i)\Big]$	Height to adjacent saddle
Landau expansion	$U(\psi) = a(T-T_c)\psi^2 + b\psi^4 + \cdots$	Curvature sign flip at T_c

7.1 Acronym Glossary

Table 3: Glossary of Common Acronyms and Symbols

Acronym	Full Expression	Context
PES	Potential Energy Surface	Multidimensional landscapes for molecules, solids, devices
TST	Transition State Theory	Rate theory at a first-order saddle on a PES
WKB	Wentzel–Kramers–Brillouin	Semiclassical tunneling approximation
NEB	Nudged Elastic Band	Minimum-energy path algorithm on a PES
JJ	Josephson Junction	Superconducting weak link forming a nonlinear potential
RCSJ	Resistively and Capacitively Shunted Junction	Dynamical model for current-biased JJs
MQT	Macroscopic Quantum Tunneling	Quantum escape of a collective coordinate (e.g., JJ phase)
SQUID	Superconducting Quantum Interference Device	Interferometric magnetometer based on JJs
MOSFET	Metal–Oxide–Semiconductor Field-Effect Transistor	Semiconductor device, band-bending control
V_{bi}	Built-in Potential	p-n junction barrier at equilibrium
W	Depletion Width	Total width $x_p + x_n$ of the space-charge region
ω_p	Plasma Frequency	Small-oscillation frequency in a JJ well
ΔU	Barrier Height	Energy difference between a well minimum and the adjacent saddle

8 Conclusion: A Representation Agnostic Vision

From the simple act of a ball rolling down a hill to the probabilistic leap of a quantum particle through a barrier, the potential energy diagram has provided physicists with a powerful and unifying way to visualize and understand the dynamics of physical systems. Its strength lies in its simplicity and its deep connection to our everyday intuition about energy and motion. By mapping abstract concepts like reaction coordinates or quantum phases onto a familiar graphical landscape, it makes the invisible visible and the complex comprehensible.

The evolution of this diagram is a story of scientific progress itself. Each new domain of physics, from classical mechanics to quantum computing, has adapted the tool for its own purposes, adding new layers of sophistication while retaining the core metaphor. We have seen how the simple hill of classical mechanics becomes the activation barrier of chemistry, the tunneling wall of quantum mechanics, the bent bands of semiconductor physics, and the tilted washboard of quantum computing. We have also explored the rigorous mathematical framework of stability that underlies these intuitive pictures.

The arrows may now point *through* the hills as often as they point *over* them, and the landscape may be a multi-dimensional, computer-generated surface rather than a simple hand-drawn curve. Yet, the fundamental idea remains unchanged. Physicists continue to rely on these gravity-inspired sketches to portray the energetic cost of crossing from “here” to “there.” Whether the traveler is a reacting molecule, a tunneling alpha particle, a drifting electron, or a macroscopic quantum phase, the diagram’s hill captures both the challenge and the creativity of the journey, proving its status as one of the most enduring and effective conceptual tools in all of science.

License